Acta Crystallographica Section F
Structural Biology and Crystallization Communications
ISSN 1744-3091

Crystallization and preliminary crystallographic studies of dihydrofolate reductase-thymidylate synthase from *Trypanosoma cruzi*, the Chagas disease pathogen

Penchit Chitnumsub,[a]* Jirundon Yuvaniyama,[b] Thippayarat Chahomchuen,[a] Tirayut Vilaivan[c] and Yongyuth Yuthavong[a]

[a]National Center for Genetic Engineering and Biotechnology, 113 Thailand Science Park, Pathumthani 12120, Thailand, [b]Department of Biochemistry and Center for Excellence in Protein Structure and Function, Faculty of Science, Mahidol University, Bangkok 10400, Thailand, and [c]Department of Chemistry, Faculty of Science, Chulalongkorn University, Bangkok 10330, Thailand

Correspondence e-mail: penchit@biotec.or.th

Received 31 August 2009
Accepted 13 October 2009

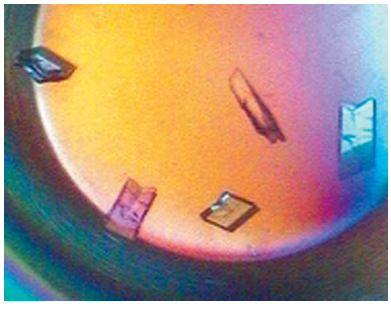

Trypanosoma cruzi dihydrofolate reductase-thymidylate synthase (TcDHFR-TS) was crystallized in complexes with the dihydrotriazine-based or quinazoline-based antifolates C-448, cycloguanil (CYC) and Q-8 in order to gain insight into the interactions of this DHFR enzyme with classical and novel inhibitors. The TcDHFR-TS–C-448–NDP–dUMP crystal belonged to space group $C222_1$ with two molecules per asymmetric unit and diffracted to 2.37 Å resolution. The TcDHFR-TS–CYC, TcDHFR-TS–CYC–NDP and TcDHFR-TS–Q-8–NDP crystals belonged to space group $P2_1$ with four molecules per asymmetric unit and diffracted to 2.1, 2.6 and 2.8 Å resolution, respectively. Crystals belonging to the two different space groups were suitable for structure determination.

1. Introduction

Chagas disease or American trypanosomiasis is a parasitic infectious disease caused by the kinetoplastid protozoan *Trypanosoma cruzi* and is one of the most serious public health problems in South and Central America (Barrett *et al.*, 2003). Only two drugs, nifurtimox (Bayer) and benznidazole (Roche), are available and these have low efficacy because of toxicity and resistance. Therefore, there is an urgent need to develop effective new drugs for the treatment of Chagas disease.

Dihydrofolate reductase (DHFR) has been a very successful target in the areas of anticancer, antibacterial and antimalarial chemotherapy (Tarnchompoo *et al.*, 2002; Sirichaiwat *et al.*, 2004; Kamchonwongpaisan *et al.*, 2004). The DHFR enzyme catalyzes the conversion of dihydrofolate (H_2F) to tetrahydrofolate (H_4F) by an NADPH-dependent reduction. *T. cruzi* DHFR exists as a bifunctional protein with the TS domain located at the C-terminus. Inhibition of DHFR or TS prevents DNA biosynthesis, leading to cell death. However, trypanosomatid protozoans such as *T. cruzi* can salvage pteridine and biopterin, which are then reduced by pteridine reductase 1 (PTR1; Bello *et al.*, 1994; Schormann *et al.*, 2001, 2008). PTR2 of *T. cruzi*, which has a similar primary sequence to PTR1, can only reduce dihydrobiopterin and dihydrofolate (Robello *et al.*, 1997; Senkovich *et al.*, 2003). Therefore, the PTR1 and PTR2 functions both partially overlap with that of DHFR and are presumably able to compensate for the loss of DHFR activity arising from inhibition by antifolate drugs. Nevertheless, Robello and coworkers demonstrated that PTR1 of *T. cruzi* is only expressed in the epimastigote forms of the parasite in the insect vector and not in the amastigote or trypomastigote forms present in the human blood stage (Robello *et al.*, 1997). Moreover, DHFR-TS has been validated as an essential target in another kinetoplastid species, *T. brucei* (Sienkiewicz *et al.*, 2008). There is therefore compelling evidence to explore TcDHFR-TS as a potential drug target for Chagas disease.

Structures of TcDHFR-TS have recently been reported in the folate-free state and in complexes with trimetrexate (TMQ) and methotrexate (MTX) (Fig. 1) at 2.4, 3.0 and 3.3 Å resolution in space groups $C222_1$, $I4_122$ and $P4_32_12$, respectively (Senkovich *et al.*, 2009; Schormann *et al.*, 2008). The quinazoline analogue TMQ and the aminopterin analogue MTX have similar structures to that of the physiological substrate DHF. Here, we have initiated investigations of the binding modes of different classes of inhibitors and report the cocrystallization and preliminary X-ray diffraction analysis of

TcDHFR-TS in complexes with Q-8, a quinazoline with different substitution, as well as cycloguanil (CYC) and its derivative C-448, which are antifolates with a triazine core. It is expected that the structural insights into TcDHFR-TS and antifolate interaction should reveal in part the molecular basis of drug affinity and binding environment and provide opportunities for the development of more effective novel inhibitors against DHFR for the treatment of Chagas disease.

2. Experimental procedures

2.1. Expression and purification of TcDHFR-TS

A single colony of *Escherichia coli* BL21 (DE3) pLysS cells transformed with pET-11c tcdhfr-ts (a gift from Dolores Gonzalez Pacanoska, Institute de Parasitologia y Biomedicina, Granada, Spain) was grown overnight with shaking at 310 K in Luria–Bertani (LB) medium with 100 µg ml^{-1} ampicillin and 34 µg ml^{-1} chloramphenicol. 6 l *E. coli* cell suspension with 1.5% inoculum from the overnight culture was grown at 310 K in LB medium containing 100 µg ml^{-1} ampicillin to mid-log phase ($OD_{600\,nm} \simeq 1.0$) and was then induced with 0.4 m*M* IPTG for an additional 5 h. Cells were collected by centrifugation at 10 500*g* for 8 min.

The cell pellets were resuspended in buffer *A* [0.1 m*M* EDTA, 10 m*M* DTT, 50 m*M* KCl, 20 m*M* potassium phosphate buffer pH 7.2, 20%(*v*/*v*) glycerol] and lysed at 69 MPa using a French Press (Thermo Dynamics Ltd). The lysate was clarified by centrifugation at 27 000*g* for 1 h. The supernatant (crude extract) was loaded onto an MTX affinity column (Bethell *et al.*, 1979; Dann *et al.*, 1976), which was then extensively washed with buffer *A* containing 1 *M* KCl until no protein was detected in the effluent; TcDHFR-TS was then eluted with 4 m*M* H_2F in buffer *B* [0.1 m*M* EDTA, 10 m*M* DTT, 50 m*M* KCl, 50 m*M* TES pH 8.2, 20%(*v*/*v*) glycerol]. DHFR-active fractions were pooled and concentrated and H_2F was removed by exchanging three times with buffer *A* by ultrafiltration at 3500*g* and 277 K using a Vivaspin-20 with 30 kDa cutoff (VivaScience, Germany). The protein concentration was determined using the Bradford protein assay with bovine serum albumin (BSA) as the standard (Bradford, 1976).

2.2. Kinetics and inhibition

2.2.1. DHFR kinetics and inhibition. DHFR activity was determined spectroscopically at 340 nm by monitoring the decline in absorption of NADPH at 298 K using a reaction molar absorptivity of 12 300 M^{-1} cm^{-1} (Hillcoat *et al.*, 1967). Activity was assayed with 100 µ*M* of both NADPH and H_2F in a 1 ml cocktail of 50 m*M* TES buffer pH 7.0 containing 75 m*M* β-mercaptoethanol and 1 mg ml^{-1} BSA in a Hewlett Packard UV–Vis spectrophotometer (HP8453) using a single-acquisition mode. The reaction was initiated with enzyme (activity of 0.01 µmol min^{-1}). Michaelis–Menten constants (K_m values) for H_2F and NADPH were calculated as described by Segal (1975). The inhibition of DHFR by antifolate inhibitors was performed in the presence of 20 µ*M* H_2F and 100 µ*M* NADPH and inhibition constants (K_i values) were calculated by curve-fitting using the nonlinear least-squares equation for competitive inhibition in *KALEIDAGRAPH* v.3.51 (Synergy Software, Reading, Pennsylvania, USA).

2.2.2. TS kinetics. TS activity was determined spectroscopically at 340 nm by monitoring the increase in absorbance arising from conversion of 5,10-methylenetetrahydrofolate (6*R*-CH_2H_4folate) to H_2F at 298 K using a reaction molar absorptivity of 6400 M^{-1} cm^{-1} (Meek *et al.*, 1985). The reaction was assayed in a 1 ml cocktail of 150 µ*M* 6*R*-CH_2H_4folate and 125 µ*M* dUMP in 50 m*M* TES buffer pH 7.4 containing 25 m*M* $MgCl_2$, 6.5 m*M* formaldehyde, 1 m*M* EDTA and 75 m*M* β-mercaptoethanol in a Hewlett Packard UV–Vis spectrophotometer (HP8453) using a multiple-acquisition mode. The reaction was initiated with either enzyme (~0.005–0.007 µmol min^{-1}) or dUMP.

2.3. Crystallization and data collection

TcDHFR-TS was crystallized at 297 K using the microbatch method (Chayen *et al.*, 1992; D'Arcy *et al.*, 1996; Chitnumsub *et al.*, 2004) in a 60-well plate (1 mm diameter at the bottom of each well) covered with 6 ml baby oil (a mixture of mineral oil, olive oil and vitamin E; PZ Cussons, Thailand). The protein–inhibitor mixture was prepared by mixing 60 µl purified TcDHFR-TS protein (18 mg ml^{-1}) in 20 m*M* potassium phosphate buffer pH 7.0 containing 0.1 m*M* EDTA, 10 m*M* DTT, 50 m*M* KCl and 20%(*v*/*v*) glycerol with 6 µl each of the following solutions: 20 m*M* NADPH, 20 m*M* dUMP and either 10 m*M* C-448, CYC or Q-8 (Fig. 1). The mixture was equilibrated on ice for 30 min to allow complete complex formation. Crystallization was set up on a microplate by first pipetting 1 µl of the protein mixture into the well layered with oil followed by 1 µl of

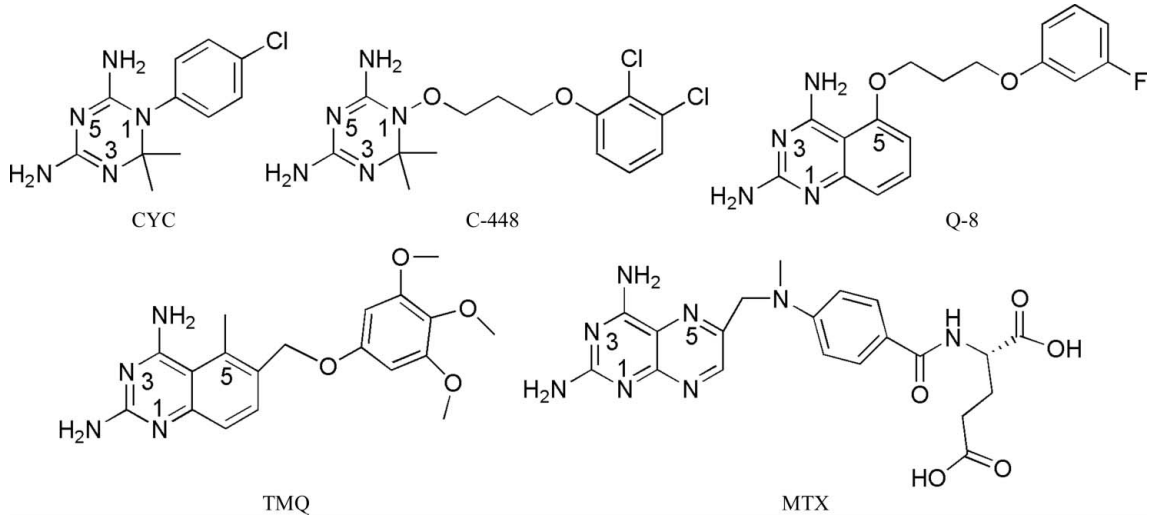

Figure 1
Antifolate structures: cycloguanil (CYC), C-448, Q-8, trimetrexate (TMQ) and methotrexate (MTX).

Table 1
Data-collection statistics for TcDHFR-TS crystals.

Values in parentheses are for the highest resolution shell.

	TcDHFR-TS –C-448–NDP –dUMP	TcDHFR-TS –CYC–NDP	TcDHFR-TS –CYC	TcDHFR-TS –Q-8–NDP
Wavelength (Å)	1.1	1.54	0.9	1.54
Space group	$C222_1$	$P2_1$	$P2_1$	$P2_1$
Molecules per ASU	2	4	4	4
Unit-cell parameters				
a (Å)	93.88	81.39	81.43	81.54
b (Å)	136.90	166.04	165.79	165.94
c (Å)	167.82	84.84	84.76	84.72
β (°)	90	113.31	113.39	113.41
Resolution (Å)	50–2.37 (2.45–2.37)	50–2.60 (2.69–2.60)	30–2.1 (2.18–2.10)	50–2.80 (2.90–2.80)
No. of measured reflections	113143	144301	308944	94398
No. of unique reflections	38355	56446	104144	45782
Redundancy	2.8	2.5	2.8	2.1
Completeness (%)	91 (85)	94 (83)	91 (80)	95 (85)
$\langle I/\sigma(I)\rangle$	12.8 (8.3)	10.6 (2.6)	10.0 (1.9)	8.7 (1.6)
$R_{\rm merge}$† (%)	6.1 (12)	7.3 (29.6)	10.3 (40.8)	9.7 (39.7)
Wilson B factor (Å^2)	35	45	31	48

† $R_{\rm merge} = \sum_{hkl}\sum_i |I_i(hkl) - \langle I(hkl)\rangle| / \sum_{hkl}\sum_i I_i(hkl)$, where $I_i(hkl)$ is the intensity of the ith measurement of an equivalent reflection with indices hkl and $\langle I(hkl)\rangle$ is the mean intensity of $I_i(hkl)$ for all i measurements.

crystallization solution, without mixing. In the initial screen at room temperature, small crystals of needle, plate and prism morphology were observed among precipitated protein in several different conditions. Optimized conditions were screened using various concentrations of ammonium acetate, ammonium sulfate, calcium chloride, lithium sulfate, sodium chloride or sodium potassium tartrate in either PEG 4000 or PEG 6000 and in the pH range 5.5–8.5.

Single crystals of the complexes were flash-vitrified in liquid nitrogen after soaking for a few seconds in the corresponding crystallization solution containing 20%(*v*/*v*) glycerol as a cryoprotectant. X-ray diffraction data were collected in a cold nitrogen stream (100 K) at a wavelength of 0.9 or 1.1 Å using a Jupiter 210 CCD detector on beamline BL38B1, SPring-8, Japan and a wavelength of 1.54 Å using a Bruker–Nonius Cu $K\alpha$ FR591 rotating-anode X-ray generator operating at 45 kV and 100 mA and equipped with a Nonius CCD detector. Data were processed using *DENZO* and *SCALEPACK* (Otwinowski & Minor, 1997) from the *HKL*-2000 package; statistics are given in Table 1. The initial phases were obtained with *AMoRe* (Navaza, 1994) in the *CCP*4 suite (Collaborative Computational Project, Number 4, 1994) using *Leishmania major* DHFR-TS as a search template.

3. Results and discussion

3.1. Purification and inhibition studies

Plasmid pET1c with a cloned *T. cruzi dhfr-ts* gene (gi:1899001) was used to transform *E. coli* BL21 (DE3) pLysS cells and expression of TcDHFR-TS was induced with 0.4 m*M* IPTG at 310 K for 5 h. TcDHFR-TS protein (58.8 kDa, 521 amino acids) was purified to homogeneity using a single MTX affinity chromatography step. The purified protein was concentrated to greater than 35 mg ml^{-1} without detectable aggregation. Protein solutions at 1 and 5 mg ml^{-1} showed a monodisperse pattern corresponding to a species with a hydrodynamic radius of 10 nm as determined using the dynamic light-scattering technique (data not shown; DynaPro, Protein Solutions). The DHFR and TS specific activities were 30.85 and 1.88 µmol min^{-1} per milligram of protein, with $k_{\rm cat}$ values of 30.26 and 1.84 s^{-1}, respectively. The Michaelis–Menten constants for H_2F and NADPH were 2.58 ± 0.22 and 7.98 ± 0.72 µ*M*, respectively. The inhibition values of C-448, Q-8 and CYC against the TcDHFR domain were 2.90 ± 0.67, 117.8 ± 6.2 and 777 ± 138 n*M*, respectively. The flexible compound C-448 was therefore a much better inhibitor than the more rigid compounds Q-8 and CYC.

3.2. Crystallization and data collection of *T. cruzi* DHFR-TS

Crystallization of TcDHFR-TS was pre-screened with a sparse matrix using the microbatch technique. Salt and polyethylene glycol (PEG) concentrations were varied in the first dimension and pH in the second dimension. TcDHFR-TS reached a high supersaturation at concentrations as low as 4 mg ml^{-1}. Microcrystal showers were obtained under several conditions. Crystals formed using a variety of salts and pH values and with either PEG 4000 or PEG 6000. Crystallization in ammonium acetate and sodium chloride in 0.1 *M* sodium citrate buffer pH 5.6 produced crystals of well defined morphology with sharp edges after optimization. Nevertheless, crystals grown using 1.2 *M* sodium chloride, 20%(*w*/*v*) PEG 4000 and 0.1 *M* sodium citrate buffer pH 5.6 only diffracted to low resolution. Unlike sodium chloride, ammonium acetate gave smaller crystals with better diffraction resolution under similar buffer conditions and PEG 4000 concentrations. Therefore, all data acquired were from crystals grown using ammonium acetate. During optimization, it was found that the crystals started to crack after 3 d. Prolonged incubation led to further cracking of the crystals (Fig. 2*c*). Therefore, data were acquired after a few days of crystallization in order to avoid high mosaicity. Because of crystal cracking and the high mosaicity, rather small crystals were selected for data collection (Fig. 2). Crystals of the complex of TcDHFR-TS with the flexible ligand (C-448) were obtained at low ionic strength, while those of complexes with the rigid ligands (CYC and Q-8) could only be grown at very high ionic strengths (Fig. 2). A TcDHFR-TS–C-448–NDP–dUMP crystal grown using 0.1–0.2 *M* ammonium acetate, 20–22%(*w*/*v*) PEG 4000 plus 0.1 *M* sodium citrate buffer pH 5.6 belonged to space group $C222_1$. Isomorphous crystals of the binary TcDHFR-TS–CYC, ternary TcDHFR-TS–CYC–NDP and ternary TcDHFR-TS–Q-8–NDP complexes were grown at ionic strengths of >0.8 *M* ammonium acetate with 20%(*w*/*v*) PEG 4000 plus 0.1 *M* sodium citrate buffer pH 5.6 and belonged to space group $P2_1$. The facts that these two crystal forms were obtained from related conditions and that the unit-cell parameters along the twofold screw axis were similar (Table 1) with similar Matthews coefficients (2.2–2.3 Å^3 Da^{-1}) and solvent contents (~45%) suggested that these crystal forms were related, possibly owing to a slight difference in ligand binding that affected the molecular packing in the lattice. This will be verified in detail after model refinements are complete. Initial phases were successfully determined with *AMoRe* in the *CCP*4 suite using *L. major* DHFR-TS as the search template. Notwithstanding the recent publications of TcDHFR-TS structures, the data presented here provide novel insights into the structure of this potential drug target. The Q-8 inhibitor in the complex reported here, despite having the same quinazoline core structure as TMQ in the previously published complex (Senkovich *et al.*, 2009), has a side-chain substitution at the 5-position instead of the 6-substitution of TMQ and formed a complex that crystallized in a different lattice. Together with the new triazine-based C-448 and CYC complexes, the X-ray diffraction data reported here are therefore expected to provide additional binding features and structural insights into the enzyme–inhibitor interactions, aiding the more precise design of new effective drugs for Chagas disease.

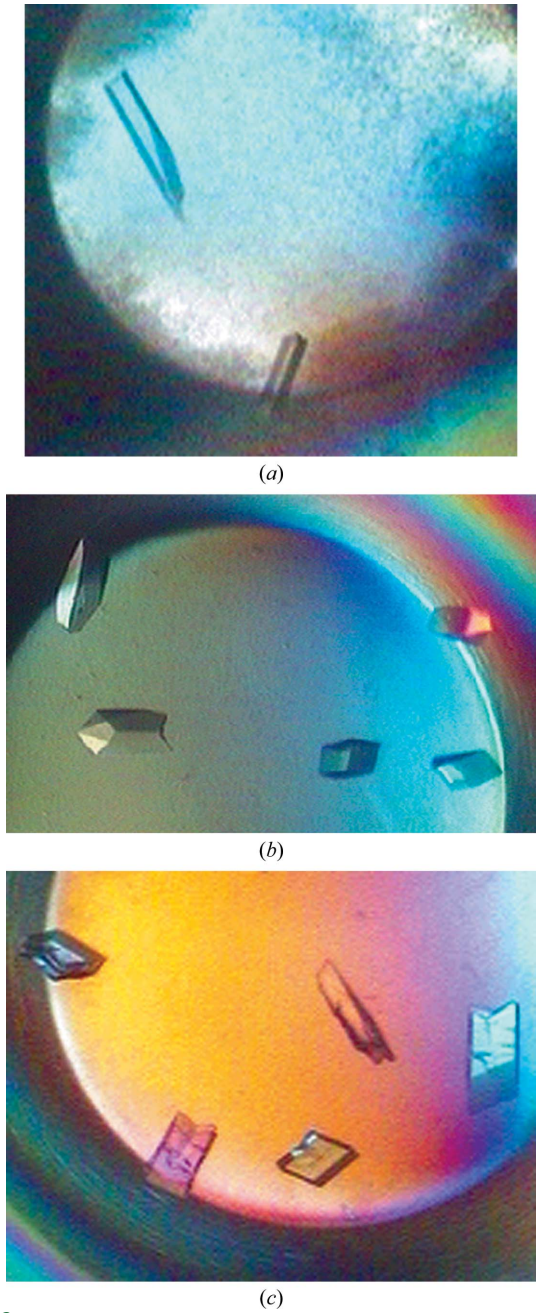

Figure 2
Crystals of TcDHFR-TS complexes. The typical dimensions of TcDHFR-TS–C-448–NDP–dUMP crystals (*a*) were 0.02 × 0.04 × 0.12 mm, while those of TcDHFR-TS–Q-8–NDP–dUMP crystals (*b*) were 0.05 × 0.05 × 0.10 mm. (*c*) The TcDHFR-TS–C-448–NDP–dUMP crystals started to crack after 3 d of equilibration.

We thank Dolores González-Pacanowska, Instituto de Parasitología y Biomedicina 'López-Neyra', Granada, Spain for the tcdhfrts plasmid, David A. Matthews for the *L. major* DHFR-TS coordinates, beamline BL38B1 at SPring-8, Japan Synchrotron Radiation Research Institute for synchrotron beam time and excellent staff support, and Target Research Unit Network (TARUN) and T2 (Thailand) for the FR591 X-ray generator. This work was supported in part by a grant from the Synchrotron Light Research Institute (Public Organization), Siam Photon Thailand (PC). We also thank Dr Arun Kumar and Ms Netnapa Charoensetakul for preparing Q-8 and C-448, respectively. The assistance of Dr Phillip Shaw in editing the manuscript is highly appreciated.

References

Barrett, M. P., Burchmore, R. J. S., Stich, A., Lazzari, J. O., Frasch, A. C., Cazzulo, J. J. & Krishna, S. (2003). *Lancet*, **362**, 1469–1480.
Bello, A. R., Nare, B., Freedman, D., Hardy, L. & Beverley, S. M. (1994). *Proc. Natl Acad. Sci. USA*, **91**, 11442–11446.
Bethell, G. S., Ayers, J. S., Hancock, W. S. & Hearn, M. T. (1979). *J. Biol. Chem.* **254**, 2572–2574.
Bradford, M. M. (1976). *Anal. Biochem.* **72**, 248–254.
Chayen, N. E., Shaw Stewart, P. D. & Blow, D. M. (1992). *J. Cryst. Growth*, **122**, 176–180.
Chitnumsub, P., Yavaniyama, J., Vanichtanankul, J., Kamchonwongpaisan, S., Walkinshaw, M. D. & Yuthavong, Y. (2004). *Acta Cryst.* D**60**, 780–783.
Collaborative Computational Project, Number 4 (1994). *Acta Cryst.* D**50**, 760–763.
D'Arcy, A., Elmore, C., Stihle, M. & Johnston, J. E. (1996). *J. Cryst. Growth*, **168**, 175–180.
Dann, J. G., Ostler, G., Bjur, R. A., King, R. W., Scudder, P., Turner, P. C., Roberts, G. C. & Burgen, A. S. (1976). *Biochem. J.* **157**, 559–571.
Hillcoat, B. L., Nixon, P. F. & Blakley, R. L. (1967). *Anal. Biochem.* **21**, 178–189.
Kamchonwongpaisan, S., Quarrell, R., Charoensetakul, N., Ponsinet, R., Vilaivan, T., Vanichtanankul, J., Tarnchompoo, B., Sirawaraporn, W., Lowe, G. & Yuthavong, Y. (2004). *J. Med. Chem.* **47**, 673–680.
Meek, T. D., Garvey, E. P. & Santi, D. V. (1985). *Biochemistry*, **24**, 678–686.
Navaza, J. (1994). *Acta Cryst.* A**50**, 157–163.
Otwinowski, Z. & Minor, W. (1997). *Methods Enzymol.* **276**, 307–326.
Robello, C., Navarro, P., Castanys, S. & Gamarro, F. (1997). *Mol. Biochem. Parasitol.* **90**, 525–535.
Schormann, N., Pal, B. & Chattopadhyay, D. (2001). *Acta Cryst.* D**57**, 1671–1673.
Schormann, N., Senkovich, O., Walker, K., Wright, D. L., Anderson, A. C., Rosowsky, A., Ananthan, S., Shinkre, B., Velu, S. & Chattopadhyay, D. (2008). *Proteins*, **73**, 889–901.
Segal, I. H. (1975). *Enzyme Kinetics: Behavior and Analysis of Steady-State and Rapid Equilibrium Enzyme Systems.* New York: Wiley-Interscience.
Senkovich, O., Pal, B., Schormann, N. & Chattopadhyay, D. (2003). *Mol. Biochem. Parasitol.* **127**, 89–92.
Senkovich, O., Schormann, N. & Chattopadhyay, D. (2009). *Acta Cryst.* D**65**, 704–716.
Sienkiewicz, N., Jaroslawski, S., Wyllie, S. & Fairlamb, A. H. (2008). *Mol. Microbiol.* **69**, 520–533.
Sirichaiwat, C., Intaraudom, C., Kamchonwongpaisan, S., Vanichtanankul, J., Thebtaranonth, Y. & Yuthavong, Y. (2004). *J. Med. Chem.* **47**, 345–354.
Tarnchompoo, B., Sirichaiwat, C., Phupong, W., Intaraudom, C., Sirawaraporn, W., Kamchonwongpaisan, S., Vanichtanankul, J., Thebtaranonth, Y. & Yuthavong, Y. (2002). *J. Med. Chem.* **45**, 1244–1252.